In summary, the structures of IL-18 and its receptor have advanced our precise understanding of molecular recognition and suggest a single architectural paradigm for signalling complexes in the IL-1 family cytokines. Furthermore, with biochemical and cellular data, the structures reveal detailed interaction properties at the molecular interfaces, presenting an atomic framework that will aid in rational drug development for IL-18-related diseases.

Methods

Construction of expression vectors. The coding region of the extracellular domains of human IL-18Rα (NM_003855, residues 20–329) and IL-18Rβ (NM_003853, residues 15–356) were cloned into the pFastBac1 vector (Invitrogen, Carlsbad, CA, USA). Full-length IL-18Rβ was also cloned into the pcDNA3.1 + vector (Invitrogen). The pGL4.32[luc2P/NF-κB-RE/Hygro] vector was used as an NF-κB luciferase reporter, and the pGL4.70[hRluc] vector was used as an internal control *Renilla* luciferase reporter; both were purchased from Promega (Fitchburg, WI, USA). For the crystallographic studies, the signal-peptide sequence for Sf9 insect cells, an 8 × His tag and an HRV 3C protease cleavage site were placed immediately upstream of the mature sequence[35]. The same constructs with a C-terminal 6 × His tag and without the HRV 3C site were also prepared for solution structure analysis and SPR experiments. Mutations were introduced into the pGEX4T-1[IL-18][19], pFastBac1[IL-18Rs] and pcDNA3.1 + [IL-18Rβ] vectors using an inverse PCR-based site-directed mutagenesis method.

Protein expression and purification. Mature IL-18 (residues 1–157) and its single amino-acid mutants were prepared as previously reported[19]. In brief, human IL-18 was expressed as a glutathione S-transferase (GST) fusion protein in the *Escherichia coli* strain BL21(DE3) (Novagen, Madison, WI, USA). GST-tagged IL-18 was affinity purified followed by GST digestion with Factor Xa and further purified using gel filtration column chromatography. Expression of IL-18Rs using Sf9 insect cell system and their detailed purification procedures were also described[35]. The extracellular human IL-18Rα or IL-18Rβ domains were each separately secreted from Sf9 insect cells (Invitrogen) for structural analyses. The supernatant was purified through three chromatography steps, including ion exchange chromatography, Ni-NTA affinity chromatography and gel filtration chromatography with or without an HRV 3C treatment. To obtain the IL-18/IL-18Rα binary and IL-18/IL-18Rα/IL-18Rβ ternary complexes, IL-18, IL-18Rα and IL-18Rβ were mixed at equimolar ratios and purified through gel filtration chromatography. Both the wild type and the mutants of the IL-18Rs for SPR analysis were expressed using a silkworm system[36,37]. The donor plasmids of the pFastBac1 vectors containing the IL-18 receptor gene were transformed into *Escherichia coli* BmDH10Bac. Then, 1 μg of BmNPV bacmid DNA and 1 μl of Cellfectin reagent (Invitrogen) suspended in Grace insect cell medium were injected into the ventral side of *B. mori* silkworm larvae. After 6 days, haemolymph was recovered from the larvae, and sodium thiosulfate (final 0.5%) and EDTA were immediately added. The IL-18 receptor proteins from the silkworm were purified using the same protocols as the purification from the Sf9 insect cell system.

Cell culture. HEK293 cells (Japanese Collection of Research Bioresources, Osaka, Japan) were cultured in Dulbecco's modified Eagle's medium (high glucose-containing D-MEM, Invitrogen) supplemented with 10% heat-inactivated fetal bovine serum (Sigma-Aldrich, Missouri, USA), penicillin (100 unit ml^{-1}) and streptomycin (100 μg ml^{-1}). All cells were incubated at 37 °C in a humidified atmosphere of 5% CO_2.

Luciferase reporter gene assay. HEK293 cells were transfected with an empty pcDNA3.1 + vector or pcDNA3.1 + [IL-18Rβ] (wild-type or mutants), pGL4.32[luc2P/NF-κB-RE/Hygro] and pGL4.70[hRluc] vectors using Lipofectamine 2000 reagent according to the manufacturer's instructions. These transfectants were stimulated with recombinant human IL-18 (10 ng ml^{-1}) for 6 h. The luciferase reporter gene activities were analysed using a Dual-Luciferase Reporter Assay System (Promega). The statistical significance of the differences was determined using one-way ANOVA with Bonferroni's multiple comparison test. The statistical significance was assigned to be $P<0.05$.

Surface plasmon resonance analysis. The real-time binding affinities between IL-18 and IL-18Rα and between IL-18Rβ and IL-18/IL-18Rα were analysed using a BIAcore 3000 surface plasmon resonance spectrometer (GE Healthcare, Little Chalfont, UK) at 25 °C with a Ni-NTA sensor chip. The K_d (dissociation constant) estimated using the Ni-NTA sensor chip was an average of one order of magnitude lower than estimates obtained using an Anti-His-tag Ab covalently linked to a CM5 sensor chip. However, we used the Ni-NTA sensor chip because it did not decrease the binding capacity after repeated measurement cycles, which is desirable when comparing the K_d of many mutants.

C-terminal 6 × His tagged IL-18Rα was immobilized approximately 200-resonance units (RU) on an NTA sensor chip. Then, various concentrations of IL-18 in HBS-P (10 mM HEPES-Na, pH7.4, 150 mM NaCl, 0.01% (v/v) surfactant P-20) buffer were injected over the sensor surface as an analyte at a flow rate of 30 μl min^{-1} for 180 s. After association, it was allowed to run for another 360 s for dissociation. In the same way, C-terminal 6 × His tagged IL-18Rβ was immobilized approximately 100 RU on the sensor chip, and un-tagged IL-18Rα that was saturated with 500 nM IL-18 in HBS-P buffer was injected. The sensor surface was regenerated with 350 mM EDTA. For the mutational analysis, mutants of IL-18, IL-18Rα and IL-18Rβ were used instead of wild type, as shown in Supplementary Table 1. The sensor chip was analysed using BIAevaluation software (GE Healthcare). Analyses with the same concentration series were performed in triplicate.

Crystal structure determination. Step by step crystallization method and preliminary crystallographic analysis were done as described[35]. X-ray diffraction data were collected at 100 K on the BL38 (IL-18) or BL44XU (IL-18/IL-18Rα) beamlines at SPring-8 (Harima, Japan) and on the BL17A beamline (IL-18/IL-18Rα/IL-18Rβ) at Photon Factory (Tsukuba, Japan). For IL-18 and IL-18/IL-18Rα, the diffraction data were processed using the XDS[38] and SCALA[39,40] software. The initial phases were determined by molecular replacement using Phaser[41] with the crystal structure of IL-18 (ref. 20) (PDB code: 3F62) as the search model. The initial phases of the binary complex were improved by NCS averaging using RESOLVE[42]. The model was further manually built using COOT[43] and refined using BUSTER[44] with autoNCS[45]. In the IL-18 and IL-18/IL-18Rα crystals, four and six copies of IL-18 and the binary complexes were observed in each ASU, respectively. The structures of these copies in the ASUs are essentially the same, so we referred to chain A for IL-18 and chain A/B for IL-18/IL-18Rα, if not otherwise indicated. The structure of IL-18 included 13 molecules of CHAPS. The diffraction data of IL-18/IL-18Rα/IL-18Rβ were processed using HKL2000 software[46]. To determine the initial phase for IL-18/IL-18Rα/IL-18Rβ, a refined structure of the binary complex was used as the search model for molecular replacement. The model was further manually built using COOT and refined using BUSTER. Only one copy of the ternary complex was in the IL-18/IL-18Rα/IL-18Rβ crystal ASU. Ramachandran diagrams were examined using RAMPAGE[47]. Structural figures were prepared using PyMol (Schrödinger, LLC). The secondary structures were assigned using the DSSP software[48].

NMR spectroscopy. All NMR spectra were measured at 308 K on a Bruker Avance II 700 MHz spectrometer equipped with cryogenic probes using TROSY-type pulse sequences. The samples for NMR measurements were in 20 mM potassium phosphate (pH 6.0), 50 mM KCl in H_2O/D_2O (90%/10%). Spectra were processed using NMRPipe[49] and analysed using Sparky analysis software[50].

Chemical shift assignments for IL-18 bound to IL-18Rα are based on a HN(CO)CA/HNCA data set and confirmed by HNCACB and NOESY spectra with a mixing time of 200 ms. The IL-18Rα binding surface of IL-18 in solution is defined by the cross-saturation[28] intensity ratio of I_{2000ms}/I_{0ms}. The IL-18Rβ binding site of IL-18 is inferred from the titration experiment, by shifted or eliminated peaks, which can be assigned for all but the IL-18Rα binding surface. Structural figures were prepared using PyMol (Schrödinger, LLC).

Small-angle X-ray scattering. SAXS data of the IL-18/IL-18Rα/IL-18Rβ ternary complex were collected at the beamline 12ID-B of the Advanced Photon Source at Argonne National Laboratory (Argonne, IL, USA). The sample concentrations were 1, 3 and 5 mg^{-1} ml^{-1}. The samples were run at 12 keV radiation energy, with a sample-to-detector distance of 2 m. The scattered X-rays were measured using a Pilatus 2 M detector. A flow cell was used to reduce radiation damage. Thirty images were taken for each blank and each sample.

After background subtraction, the data were superimposed using Primus[51] (Supplementary Fig. 4f). S is the momentum transfer equal to $4\pi\sin(\theta/2)/\lambda$, where θ and λ are the scattering angle and X-ray wavelength, respectively. R_g is the radius of gyration, which was determined using the Guinier approximation of the data in the low s region ($sR_g<1.3$), the linearity of which also served as an initial assessment of data quality (Supplementary Fig. 4g). The maximum particle dimension, D_{max}, and the distance distribution function, $P(r)$, were calculated using auto GNOM[52] (Supplementary Fig. 4h). The low-resolution envelopes of the ternary complex were produced using DAMMIN[53] by directly fitting the reciprocal space scattering profile. Fifteen DAMMIN models were generated and then aligned and averaged using DAMAVER and DAMFILT[54]. Structural figures were prepared using Chimera[55].

References

1. Okamura, H. *et al.* Cloning of a new cytokine that induces IFN-gamma production by T cells. *Nature* **378,** 88–91 (1995).
2. Kuida, K. *et al.* Altered cytokine export and apoptosis in mice deficient in interleukin-1 beta converting enzyme. *Science* **267,** 2000–2003 (1995).
3. Li, P. *et al.* Mice deficient in IL-1 beta-converting enzyme are defective in production of mature IL-1 beta and resistant to endotoxic shock. *Cell* **80,** 401–411 (1995).

4. Ghayur, T. *et al.* Caspase-1 processes IFN-gamma-inducing factor and regulates LPS-induced IFN-gamma production. *Nature* **386,** 619–623 (1997).
5. Rathinam, V. a. K., Vanaja, S. K. & Fitzgerald, K. a. Regulation of inflammasome signaling. *Nat. Immunol.* **13,** 333–2 (2012).
6. Ohnishi, H. *et al.* TRAM is involved in IL-18 signaling and functions as a sorting adaptor for MyD88. *PLoS ONE* **7,** e38423 (2012).
7. Adachi, O. *et al.* Targeted disruption of the MyD88 gene results in loss of IL-1- and IL-18-mediated function. *Immunity* **9,** 143–150 (1998).
8. Hoffman, H. M., Mueller, J. L., Broide, D. H., Wanderer, A. A. & Kolodner, R. D. Mutation of a new gene encoding a putative pyrin-like protein causes familial cold autoinflammatory syndrome and Muckle-Wells syndrome. *Nat. Genet.* **29,** 301–305 (2001).
9. Park, H., Bourla, A. B., Kastner, D. L., Colbert, R. a. & Siegel, R. M. Lighting the fires within: the cell biology of autoinflammatory diseases. *Nat. Rev. Immunol.* **12,** 570–580 (2012).
10. Dinarello, C. a., Simon, A. & van der Meer, J. W. M. Treating inflammation by blocking interleukin-1 in a broad spectrum of diseases. *Nat. Rev. Drug Discov.* **11,** 633–652 (2012).
11. Alboni, S., Cervia, D., Sugama, S. & Conti, B. Interleukin 18 in the CNS. *J. Neuroinflamm.* **7,** 9 (2010).
12. Mellins, E. D., Macaubas, C. & Grom, A. A. Pathogenesis of systemic juvenile idiopathic arthritis: some answers, more questions. *Nat. Rev. Rheumatol.* **7,** 416–426 (2011).
13. Hirota, T. *et al.* Genome-wide association study identifies eight new susceptibility loci for atopic dermatitis in the Japanese population. *Nat. Genet.* **44,** 1222–1226 (2012).
14. Dinarello, C. A., Novick, D., Kim, S. & Kaplanski, G. Interleukin-18 and IL-18 binding protein. *Front. Immunol.* **4,** 289 (2013).
15. Romberg, N. *et al.* Mutation of NLRC4 causes a syndrome of enterocolitis and autoinflammation. *Nat. Genet.* **46,** 1135–1139 (2014).
16. Canna, S. W. *et al.* An activating NLRC4 inflammasome mutation causes autoinflammation with recurrent macrophage activation syndrome. *Nat. Genet.* **46,** 1140–1146 (2014).
17. Terada, M. *et al.* Contribution of IL-18 to atopic-dermatitis-like skin inflammation induced by Staphylococcus aureus product in mice. *Proc. Natl Acad. Sci. USA* **103,** 8816–8821 (2006).
18. Brydges, S. D. *et al.* Divergence of IL-1, IL-18, and cell death in NLRP3 inflammasomopathies. *J. Clin. Invest.* **123,** 4695–4705 (2013).
19. Kato, Z. *et al.* The structure and binding mode of interleukin-18. *Nat. Struct. Biol.* **10,** 966–971 (2003).
20. Krumm, B., Meng, X., Li, Y., Xiang, Y. & Deng, J. Structural basis for antagonism of human interleukin 18 by poxvirus interleukin 18-binding protein. *Proc. Natl Acad. Sci. USA* **105,** 20711–20715 (2008).
21. Argiriadi, M. A., Xiang, T., Wu, C., Ghayur, T. & Borhani, D. W. Unusual water-mediated antigenic recognition of the proinflammatory cytokine interleukin-18. *J. Biol. Chem.* **284,** 24478–24489 (2009).
22. Krumm, B., Meng, X., Wang, Z., Xiang, Y. & Deng, J. A unique bivalent binding and inhibition mechanism by the yatapoxvirus interleukin 18 binding protein. *PLoS Pathog.* **8,** e1002876 (2012).
23. Wang, D. *et al.* Structural insights into the assembly and activation of IL-1β with its receptors. *Nat. Immunol.* **11,** 905–911 (2010).
24. Thomas, C., Bazan, J. F. & Garcia, K. C. Structure of the activating IL-1 receptor signaling complex. *Nat. Struct. Mol. Biol.* **19,** 455–457 (2012).
25. Liu, X. *et al.* Structural insights into the interaction of IL-33 with its receptors. *Proc. Natl. Acad. Sci. USA* **110,** 14918–14923 (2013).
26. Vigers, G. P., Anderson, L. J., Caffes, P. & Brandhuber, B. J. Crystal structure of the type-I interleukin-1 receptor complexed with interleukin-1beta. *Nature* **386,** 190–194 (1997).
27. Günther, S. & Sundberg, E. J. Molecular determinants of agonist and antagonist signaling through the IL-36 receptor. *J. Immunol.* **193,** 921–930 (2014).
28. Takahashi, H., Nakanishi, T., Kami, K., Arata, Y. & Shimada, I. A novel NMR method for determining the interfaces of large protein-protein complexes. *Nat. Struct. Biol.* **7,** 220–223 (2000).
29. Garlanda, C., Dinarello, C. a. & Mantovani, A. The interleukin-1 family: back to the future. *Immunity* **39,** 1003–1018 (2013).
30. Park, E. Y. *et al.* Human IgG1 expression in silkworm larval hemolymph using BmNPV bacmids and its N-linked glycan structure. *J. Biotechnol.* **139,** 108–114 (2009).
31. Nold, M. F. *et al.* IL-37 is a fundamental inhibitor of innate immunity. *Nat. Immunol.* **11,** 1014–1022 (2010).
32. Kumar, S. *et al.* Interleukin-1F7B (IL-1H4/IL-1F7) is processed by caspase-1 and mature IL-1F7B binds to the IL-18 receptor but does not induce IFN-gamma production. *Cytokine* **18,** 61–71 (2002).
33. Hamasaki, T. *et al.* Human anti-human IL-18 antibody recognizing the IL-18-binding site 3 with IL-18 signaling blocking activity. *J. Biochem.* **138,** 433–442 (2005).
34. Kim, S. H. *et al.* Site-specific mutations in the mature form of human IL-18 with enhanced biological activity and decreased neutralization by IL-18 binding protein. *Proc. Natl Acad. Sci. USA* **98,** 3304–3309 (2001).
35. Kimura, T. *et al.* Purification, crystallization and preliminary X-ray crystallographic analysis of human IL-18 and its extracellular complexes. *Acta Crystallogr. Sect. F, Struct. Biol. Commun.* **70,** 1351–1356 (2014).
36. Motohashi, T., Shimojima, T., Fukagawa, T., Maenaka, K. & Park, E. Y. Efficient large-scale protein production of larvae and pupae of silkworm by Bombyx mori nuclear polyhedrosis virus bacmid system. *Biochem. Biophys. Res. Commun.* **326,** 564–569 (2005).
37. Kajikawa, M. *et al.* Silkworm Baculovirus Expression System for Molecular Medicine. *J. Biotechnol. Biomater.* **S9,** 1–5 (2012).
38. Kabsch, W. Xds.. *Acta Crystallogr. D. Biol. Crystallogr.* **66,** 125–132 (2010).
39. Evans, P. Scaling and assessment of data quality. *Acta Crystallogr. D. Biol. Crystallogr.* **62,** 72–82 (2006).
40. Evans, P. R. An introduction to data reduction: space-group determination, scaling and intensity statistics. *Acta Crystallogr. D. Biol. Crystallogr.* **67,** 282–292 (2011).
41. McCoy, A. J. *et al.* Phaser crystallographic software. *J. Appl. Crystallogr.* **40,** 658–674 (2007).
42. Terwilliger, T. C. Statistical density modification with non-crystallographic symmetry. *Acta Crystallogr. D. Biol. Crystallogr.* **58,** 2082–2086 (2002).
43. Emsley, P. & Cowtan, K. Coot: model-building tools for molecular graphics. *Acta Crystallogr. D. Biol. Crystallogr.* **60,** 2126–2132 (2004).
44. Bricogne, G. *et al.* BUSTER. 2.10.0 Ed., Global Phasing Ltd, UK (2011).
45. Smart, O. S. *et al.* Exploiting structure similarity in refinement: automated NCS and target-structure restraints in BUSTER. *Acta Crystallogr. D. Biol. Crystallogr.* **68,** 368–380 (2012).
46. Otwinowski, Z. & Minor, W. Processing of X-ray diffraction data collected in oscillation mode. *Methods Enzymol.* **276,** 307–326 (1997).
47. Lovell, S. C. *et al.* Structure validation by Calpha geometry: phi,psi and Cbeta deviation. *Proteins* **50,** 437–450 (2003).
48. Joosten, R. P. *et al.* A series of PDB related databases for everyday needs. *Nucleic Acids Res.* **39,** D411–D419 (2011).
49. Delaglio, F. *et al.* NMRPipe: a multidimensional spectral processing system based on UNIX pipes. *J. Biomol. NMR* **6,** 277–293 (1995).
50. Lee, W., Westler, W. M., Bahrami, A., Eghbalnia, H. R. & Markley, J. L. PINE-SPARKY: graphical interface for evaluating automated probabilistic peak assignments in protein NMR spectroscopy. *Bioinformatics* **25,** 2085–2087 (2009).
51. Konarev, P. V., Volkov, V. V., Sokolova, A. V., Koch, M. H. J. & Svergun, D. I. PRIMUS: a Windows PC-based system for small-angle scattering data analysis. *J. Appl. Crystallogr.* **36,** 1277–1282 (2003).
52. Svergun, D. I. Determination of the regularization parameter in indirect-transform methods using perceptual criteria. *J. Appl. Crystallogr.* **25,** 495–503 (1992).
53. Svergun, D. I. Restoring low resolution structure of biological macromolecules from solution scattering using simulated annealing. *Biophys. J.* **76,** 2879–2886 (1999).
54. Volkov, V. V. & Svergun, D. I. Uniqueness of ab initio shape determination in small-angle scattering. *J. Appl. Crystallogr.* **36,** 860–864 (2003).
55. Pettersen, E. F. *et al.* UCSF Chimera-a visualization system for exploratory research and analysis. *J. Comput. Chem.* **25,** 1605–1612 (2004).

Acknowledgements

X-ray data collection was supported by SPring-8 (Harima, Japan), Photon Factory (Tsukuba, Japan), Argonne National Laboratory (Illinois, USA, supported by DE-AC02-06CH11357) and Platform for Drug Discovery, Informatics, and Structural Life Science (Japan). We thank T. Tsunaka (Kyoto University) for the use of his beam time of BL44XU at SPring-8. We also thank T. Fukao, N. Kawamoto, K. Tsuji, M. Yamamoto, S. Ninomiya, T. Yano and K. Kasahara (Gifu University) for their scientific advice or technical help. Affymetrix, Inc. provided discontinued detergents to us. SAXS graphics were prepared using the UCSF Chimera package, which developed by the group at the University of California. (San Francisco, USA, supported by NIGMS P41-GM103311). This work was supported by JSPS KAKENHI Grant Number 22370038 to H.T., Grant-in-Aid for JSPS Fellows to N.T., Health and Labour Science Research Grants for Research on Intractable Diseases from the Ministry of Health, Labour and Welfare to H.O., Health and Labour Science Research Grants for Research from the Ministry of Health, Labour and Welfare to Z.K., Science Research Grant from Eishukai to Z.K, and MEXT KAKENHI Grant Number 21790979 to T.K.

Author contributions

H.T. and Z.K. designed the work; M.S and N.K. supervised the study; N.T. carried out the experimental design, experiments and structural analyses, supported by T.K., K.A., M.A. and H.T.; T.K. prepared the samples for the study, supported by H.O., N.T., K.M. and E.Y.P.; T.K. performed and analysed the SPR experiments; T.Y. performed the cell assays,

supported by H.O. and T.K.; X.Z. performed the SAXS measurements; and N.T., T.K., K.A., H.O., Z.K. and H.T. contributed to writing the manuscripts and preparing the figures.

Additional information

Accession codes: The atomic coordinates and structure factors for IL-18, IL-18/IL-18Rα and IL-18/IL-18Rα/IL-18Rβ have been deposited in the RCSB Protein Data Bank under accession codes 3WO2, 3WO3 and 3WO4, respectively.

Supplementary Information accompanies this paper at http://www.nature.com/naturecommunications

Competing financial interests: The authors declare no competing financial interests.

Reprints and permission information is available online at http://npg.nature.com/reprintsandpermissions/

How to cite this article: Tsutsumi, N. *et al.* The structural basis for receptor recognition of human interleukin-18. *Nat. Commun.* 5:5340 doi: 10.1038/ncomms6340 (2014).

OPEN ACCESS
CellPress

Cell Reports
Report

XIAP Restricts TNF- and RIP3-Dependent Cell Death and Inflammasome Activation

Monica Yabal,[1] Nicole Müller,[1] Heiko Adler,[2] Nathalie Knies,[3] Christina J. Groß,[3] Rune Busk Damgaard,[4,10] Hirokazu Kanegane,[5] Marc Ringelhan,[6] Thomas Kaufmann,[7] Mathias Heikenwälder,[6] Andreas Strasser,[8,9] Olaf Groß,[3] Jürgen Ruland,[3] Christian Peschel,[1] Mads Gyrd-Hansen,[4,10] and Philipp J. Jost[1,*]

[1]III. Medizinische Klink, Klinikum rechts der Isar, Technische Universität München, 81675 München, Germany
[2]Research Unit Gene Vectors, Helmholtz Zentrum München-German Research Center for Environmental Health, GmbH, 85764 Oberschleissheim, Germany
[3]Institut für Klinische Chemie und Pathobiochemie, Klinikum rechts der Isar, Technische Universität München, 81675 München, Germany
[4]Novo Nordisk Foundation Center for Protein Research, Faculty of Health and Medical Sciences, University of Copenhagen, 2200 Copenhagen, Denmark
[5]Department of Pediatrics, Graduate School of Medicine and Pharmaceutical Sciences, University of Toyama, 2630 Sugitani, Toyama 930-0194, Japan
[6]Institute of Virology, Technische Universität München and Helmholtz Zentrum München, 81675 München, Germany
[7]Institute of Pharmacology, University of Bern, 3010 Bern, Switzerland
[8]The Walter and Eliza Hall Institute of Medical Research, Parkville,VIC 3052, Australia
[9]Department of Medical Biology, University of Melbourne, Melbourne, VIC 3052, Australia
[10]Present address: Ludwig Cancer Research, Nuffield Department of Clinical Medicine, University of Oxford, Oxford OX3 7DQ, UK
*Correspondence: philipp.jost@lrz.tum.de
http://dx.doi.org/10.1016/j.celrep.2014.05.008

SUMMARY

X-linked inhibitor of apoptosis protein (XIAP) has been identified as a potent regulator of innate immune responses, and loss-of-function mutations in XIAP cause the development of the X-linked lymphoproliferative syndrome type 2 (XLP-2) in humans. Using gene-targeted mice, we show that loss of XIAP or deletion of its RING domain lead to excessive cell death and IL-1β secretion from dendritic cells triggered by diverse Toll-like receptor stimuli. Aberrant IL-1β secretion is TNF dependent and requires RIP3 but is independent of cIAP1/cIAP2. The observed cell death also requires TNF and RIP3 but proceeds independently of caspase-1/caspase-11 or caspase-8 function. Loss of XIAP results in aberrantly elevated ubiquitylation of RIP1 outside of TNFR complex I. Virally infected Xiap$^{-/-}$ mice present with symptoms reminiscent of XLP-2. Our data show that XIAP controls RIP3-dependent cell death and IL-1β secretion in response to TNF, which might contribute to hyperinflammation in patients with XLP-2.

INTRODUCTION

X-linked inhibitor of apoptosis protein (XIAP) is an antiapoptotic protein that inhibits induction of cell death in response to intrinsic as well as extrinsic apoptotic stimuli (Gyrd-Hansen and Meier, 2010; Jost et al., 2009). Inhibition of apoptosis by XIAP is mediated by inhibiting caspase-3 and caspase-7 via its N-terminal baculoviral IAP repeat (BIR) domains (Deveraux et al., 1997). The first characterization of *Xiap*$^{-/-}$ mice showed no obvious phenotype (Olayioye et al., 2005), whereas recent studies have demonstrated a reduced capacity of *Xiap*$^{-/-}$ mice to clear certain infectious pathogens (Bauler et al., 2008; Prakash et al., 2010). In addition, the RING domain and the BIR2 domain of XIAP have been implicated in nuclear factor-κB (NF-κB) and mitogen-activated protein kinase (MAPK) signaling in response to activation of nucleotide-binding oligomerization domain 1 (NOD1) and NOD2 (Damgaard et al., 2012, 2013).

To date, XIAP has not been implicated in tumor necrosis factor (TNF)/TNF receptor (TNFR) signaling despite a well-defined role for its close IAP family members, cellular inhibitor of apoptosis proteins 1 and 2 (cIAP1/cIAP2), in this pathway (Gyrd-Hansen and Meier, 2010). cIAP1/cIAP2-dependent K63 ubiquitylation of receptor-interacting protein 1 (RIP1) after TNF stimulation provides a prosurvival signaling platform allowing for the induction of NF-κB and MAPK signaling (Bertrand et al., 2008). Loss of cIAP1/cIAP2 or deubiquitylation of RIP1 coincides with the formation of secondary TNFR signaling complexes (TNF-RSCs) that trigger cell death either through caspase-8-mediated apoptosis or through RIP3- and MLKL-dependent necroptosis (Murphy et al., 2013; O'Donnell et al., 2011; Vince et al., 2007).

There are indications that elevated necroptosis contributes to inflammation and tissue damage, at least in part, mediated by interleukin-1β (IL-1β) (Günther et al., 2011; Kang et al., 2013). IL-1β is an evolutionarily conserved cytokine that potently mediates innate and adaptive immune responses, and its deregulation causes several autoinflammatory diseases (Lamkanfi and Dixit, 2012). IL-1β is translated as an inactive proform and requires processing into bioactive IL-1β by the inflammasome (Martinon et al., 2002).

Mutations within *BIRC4* (XIAP) have been identified as the genetic cause of the X-linked lymphoproliferative syndrome type 2 (XLP-2). The mutations mostly affect the C-terminal RING domain or result in complete loss of protein expression (Damgaard et al., 2013; Marsh et al., 2010; Pachlopnik Schmid et al., 2011). Clinical symptoms are mostly attributed to the aberrant activation of macrophages and dendritic cells (DCs) and the accumulation of activated T lymphocytes often in response to viral infection (Marsh et al., 2010). This hyperactivation of immune cells results in elevated systemic levels of proinflammatory cytokines, such as IL-1β, interferon-γ (IFNγ), TNF, IL-6, and IL-18 (Marsh et al., 2010; Rigaud et al., 2006; Wada et al., 2014).

We demonstrate here an unexpected function of XIAP in curtailing excessive TNF-induced inflammasome activation. This function was independent of cIAP1/cIAP2 and restricted IL-1β production in a RIP3-dependent manner. Viral infection of *Xiap*$^{-/-}$ mice resulted in a hyperinflammatory phenotype similar to that observed in patients with XLP-2, indicating that exaggerated IL-1β secretion might contribute to XLP-2 pathogenesis.

RESULTS

TLR Activation Induces Exaggerated IL-1β Secretion in *Xiap*$^{-/-}$ and *Xiap*$^{\Delta RING}$ Dendritic Cells

XLP-2 pathology in patients is mostly ascribed to a severe hyperinflammation in response to microbial infections. We therefore hypothesized that microbial ligands trigger deregulated immune responses in *Xiap*$^{-/-}$ mice. To study cytokine responses, we differentiated dendritic cslls (DCs) from bone marrow progenitors (BMDCs) of mice lacking XIAP or expressing a knockin allele of a RING-deleted version of XIAP termed *Xiap*$^{\Delta RING}$ (*Xiap* $^{\Delta RING/\Delta RING}$) (Olayioye et al., 2005; Schile et al., 2008) (Figure S1A). After treatment with ligands for Toll-like receptor 3 (TLR3), TLR4, and TLR9, we observed a significant increase of IL-1β secretion from *Xiap*$^{-/-}$ and *Xiap*$^{\Delta RING}$ BMDCs compared to wild-type (WT) BMDCs. Whereas TNF secretion from *Xiap*$^{-/-}$ and *Xiap*$^{\Delta RING}$ cells was comparable to WT, the exaggerated IL-1β secretion correlated with increased cell death (Figure 1A). A similar phenotype was also observed in bone marrow-derived macrophages (BMDMs) (Figure S1B). IL-1β secretion and cell death, measured by a decrease of intracellular ATP levels or lactate dehydrogenase (LDH) release, occurred between 4 and 8 hr of lipopolysaccharide (LPS) exposure only in *Xiap*$^{-/-}$ BMDCs (Figure 1B). However, NF-κB and MAPK signaling and subsequent gene induction were largely identical in both genotypes (*Xiap*$^{-/-}$ and WT) in response to LPS, despite a minor elevation of phosphorylated p38 in *Xiap*$^{-/-}$ cells (Figures 1C and S1C). The elevated secretion of IL-1β in *Xiap*$^{-/-}$ BMDCs in response to LPS was remarkable because conventional inflammasome activation requires a priming and an activating signal, such as ATP, for inflammasome formation (Gross et al., 2012; Martinon et al., 2002). The hypersecretion of IL-1β correlated with the formation of conventional inflammasome complexes as shown by accumulation of NOD-like receptor family pyrin domain-containing 3 (NLRP3), Apoptosis-associated Speck-like protein containing a CARD (ASC), and caspase-1 within the NP-40-insoluble fraction only in *Xiap*$^{-/-}$ cells, but not in WT cells treated with LPS only (Figure 1D). WT BMDCs recruited ASC and caspase-1 into the NP-40 fraction only after treatment with LPS plus ATP (Figure 1D). We also observed recruitment of caspase-8 into the NP-40 fraction in *Xiap*$^{-/-}$ cells but not in WT cells after LPS treatment (Figure 1D). Immunofluorescence microscopy further confirmed ASC/caspase-1 speck formation in *Xiap*$^{-/-}$ BMDCs treated with LPS only (Figure 1E), whereas speck formation in WT cells required the addition of ATP or nigericin (Gross et al., 2012) (Figures 1D and 1E).

Of note, conventional inflammasome activation in response to ATP (Figure S1D) or nigericin (Figure 1E), and inflammasome inhibition by blocking potassium efflux or by caspase inhibition (Figure S1E), was identical in WT and *Xiap*$^{-/-}$ BMDCs. Together, this demonstrated that the priming signal alone induced substantial inflammasome formation and IL-1β secretion in *Xiap*$^{-/-}$ BMDCs, but not in WT BMDCs.

Because necrotic cell death can activate the inflammasome (Lamkanfi and Dixit, 2012), we examined the connection between IL-1β secretion and cell death. To characterize the contribution of damage-associated molecular pattern molecules (DAMPs) released from dying cells to the IL-1β secretion observed, we costimulated BMDCs with LPS plus lysates from dead cells generated by repeated freeze-thaw cycles. This treatment failed to further enhance IL-1β secretion after LPS (Figure S1F). In addition, we cocultured WT and *Xiap*$^{-/-}$ BMDCs prior to LPS stimulation. Supporting a DAMP-independent cause of inflammasome activation, we observed caspase-1 specks only in *Xiap*$^{-/-}$ cells, whereas directly adjacent WT cells did not contain specks (Figure S1G). Our data argue that cell-intrinsic signaling aberrations in *Xiap*$^{-/-}$ and *Xiap*$^{\Delta RING}$ BMDCs resulted in increased inflammasome formation.

Similar to the systemic cytokinemia observed in patients with XLP-2, we hypothesized that activation of the innate immune system might drive an exaggerated inflammatory response. This was confirmed in a murine model of acute peritonitis elicited by intraperitoneal (i.p.) injection of LPS or the adjuvant alum, which both resulted in increased IL-1β levels in the peritoneal fluid of *Xiap*$^{-/-}$ mice when compared to WT (Figures 1F and 1G). These data show that TLR stimulation of DCs caused elevated inflammasome formation and IL-1β secretion in vitro and in vivo when XIAP was missing.

IL-1β Secretion in Response to LPS in *Xiap*$^{-/-}$ BMDCs Is Mediated by TNF Signaling

We next examined what factors control the IL-1β secretion in *Xiap*$^{-/-}$ cells. IL-1β secretion was reduced by caspase-1 inhibitor treatment (YVAD), whereas an IL-1β receptor antagonist (IL-1RA; anakinra) did not substantially reduce IL-1β levels in *Xiap*$^{-/-}$ BMDCs, although some reduction was seen in *Xiap*$^{\Delta RING}$ cells (Figure S2A). This argues against a prominent role for autocrine or paracrine IL-1 receptor signaling. In contrast, anti-TNF-α (Enbrel) potently inhibited IL-1β secretion, reduced cell death, and blocked processing of caspase-8 in *Xiap*$^{-/-}$ and *Xiap*$^{\Delta RING}$ BMDCs (Figures S2A and S2B).

In line with a possible role of XIAP in regulating signaling events downstream of TNF/TNFR, we observed elevated IL-1β secretion and cell death in *Xiap*$^{-/-}$ and *Xiap*$^{\Delta RING}$ BMDCs in response to recombinant TNF (Figure 2A). This was interesting because XIAP has not been directly implicated in TNF/TNFR signal

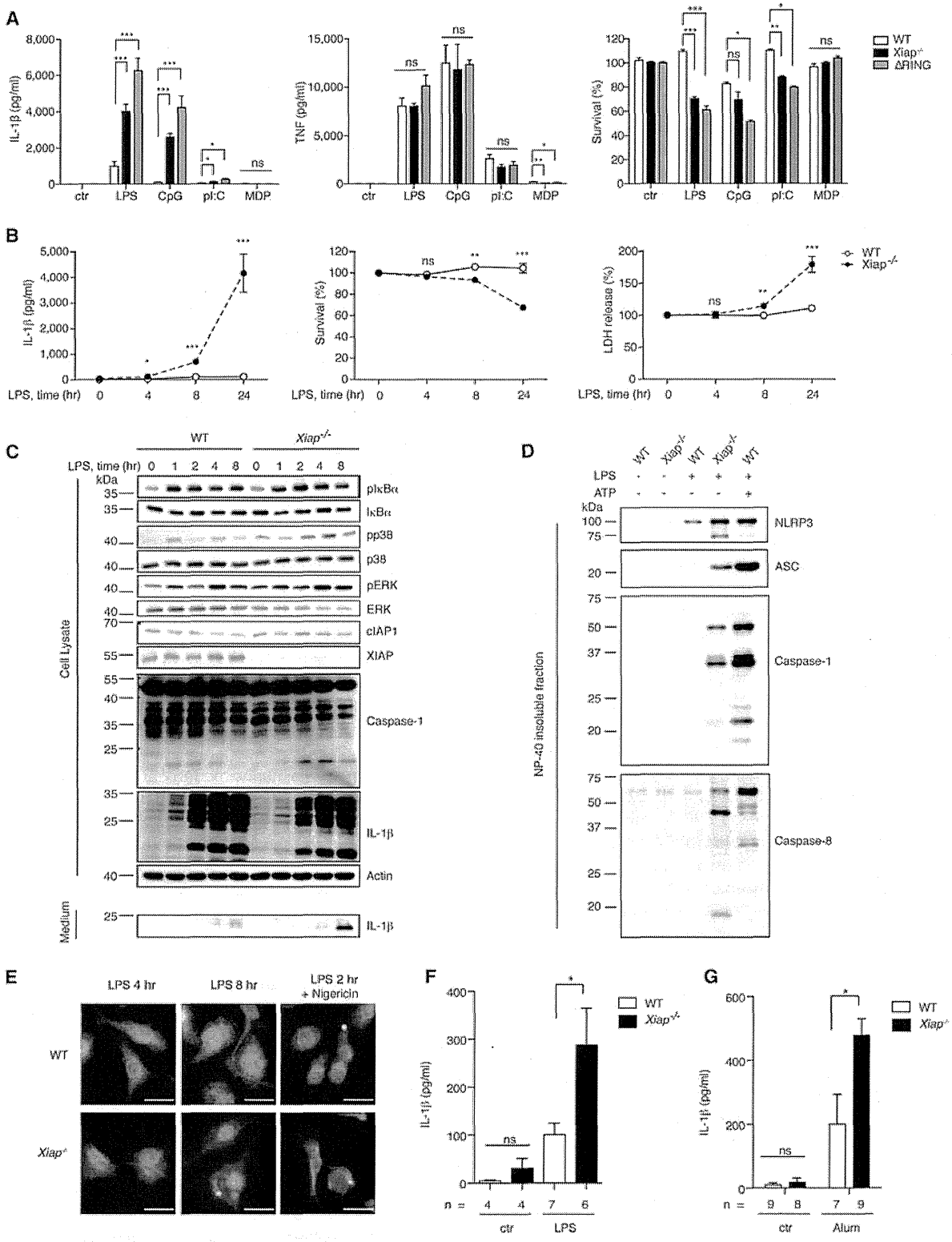

Figure 1. Exaggerated IL-1β Secretion in *Xiap*$^{-/-}$ and *Xiap*$^{\Delta RING}$ BMDCs and Mice

(A) Secreted IL-1β, TNF, and survival of WT, *Xiap*$^{-/-}$, and *Xiap*$^{\Delta RING}$ BMDCs treated with LPS, CpG (250 nM), polyI:C (10 μg/ml), or Muramyl dipeptide (MDP) (10 μg/ml) for 24 hr. ctr, control; ns, not significant.

(legend continued on next page)

transduction. Of note, we did not observe significant changes in NF-κB or MAPK signaling and gene induction in response to TNF in *Xiap*$^{-/-}$ and *Xiap*$^{\Delta RING}$ BMDCs (Figures S2C and S2D).

To better define the role of XIAP in the control of TNF signaling, we intercrossed *Xiap*$^{-/-}$ mice with mice deficient for TNF (*Tnf*^{tm1Gkl}) (Pasparakis et al., 1996). BMDCs from *Tnf*$^{-/-}$*Xiap*$^{-/-}$ double-deficient mice differentiated normally in culture (Figure S2E). Supporting a critical role of TNF/TNFR signaling for the observed phenotype, we found that genetic deletion of TNF reduced IL-1β secretion to WT levels after LPS (Figure 2B). Exogenous addition of recombinant TNF to *Tnf*$^{-/-}$*Xiap*$^{-/-}$ BMDCs fully recapitulated the excessive IL-1β production observed in *Xiap*$^{-/-}$ cells (Figure 2B). Deletion of TNF also rescued *Xiap*$^{-/-}$ BMDCs from cell death, implicating TNF-induced signaling events in both inflammasome activation and cell death (Figure 2B). Importantly, canonical inflammasome activation with ATP after a short priming stimulus with LPS caused normal inflammasome activation in *Tnf*$^{-/-}$ and *Tnf*$^{-/-}$*Xiap*$^{-/-}$ BMDCs (Figure S2F). This is in agreement with a previous report that showed that TNFR signaling was not required for canonical IL-1β maturation in response to a priming and activating signal when all IAPs were antagonized (Vince et al., 2012).

To understand the contribution of XIAP to IL-1β secretion and lymphoproliferation in vivo, we analyzed mice immunized with antigen-coated alum after 12 days. Alum induces a sustained inflammatory response primarily driven by NLRP3 inflammasome activation in inflammatory CD11c^{+} DCs (Eisenbarth et al., 2008; Kool et al., 2008). We observed an elevated splenic infiltration of inflammatory cells, such as neutrophils, macrophages, and eosinophils, in *Xiap*$^{-/-}$ mice when compared to WT mice (Jordan et al., 2004) (Figure 2C), which is reminiscent of the splenomegaly observed in many patients with XLP-2. In support of a critical role for TNF/TNFR signaling, we observed that the exaggerated splenic infiltration in *Xiap*$^{-/-}$ mice was absent in *Tnf*$^{-/-}$*Xiap*$^{-/-}$ mice (Figure 2C).

These data demonstrated that XIAP controls signaling events downstream of TNF/TNFR and thereby protects from aberrant inflammasome formation and cell death. The largely identical phenotype observed in both *Xiap*$^{\Delta RING}$ and *Xiap*$^{-/-}$ BMDCs implicated that XIAP functions as a ubiquitin ligase in this context.

Protection from Excessive Inflammasome Activation and Cell Death Is Predominantly Mediated by XIAP

Cell death triggered by TNF is often a consequence of deregulated ubiquitylation of RIP1 (Vandenabeele et al., 2010). cIAP1/cIAP2 are ubiquitin ligases of RIP1 and have been shown to protect from aberrant IL-1β secretion after TLR4 activation (Vince et al., 2012). To delineate the roles of cIAP1/cIAP2, from those of XIAP, we utilized the small molecule monovalent IAP antagonist (SMAC mimetic) LCL161. This compound has a higher affinity for cIAP1/cIAP2 than for XIAP and causes rapid degradation only of cIAP1/cIAP2, but not of XIAP (Figure 2D) (Weisberg et al., 2010).

cIAP1/cIAP2 depletion by LCL161 at 50 nM readily induced IL-1β secretion and cell death only in *Xiap*$^{-/-}$ cells, but not in WT cells (Figure 2E). Upon stimulation with LPS, WT cells depleted of cIAP1/cIAP2 failed to increase IL-1β secretion up to doses of 500 nM LCL161 (Figure 2F). In contrast, depletion of cIAP1/cIAP2 potently increased IL-1β secretion in *Xiap*$^{-/-}$ cells (Figure 2F). Interestingly, the IL-1β production was mostly TNF/TNFR dependent because *Tnf*$^{-/-}$ and *Tnf*$^{-/-}$*Xiap*$^{-/-}$ cells secreted significantly less IL-1β compared to WT and *Xiap*$^{-/-}$ cells, respectively (Figure 2F). A TNF-independent contribution to IL-1β secretion and cell death was observed only at LCL161 doses higher than 50 nM (Figure 2F).

To exclude the possibility that depletion of cIAP1 by LCL161 in *Xiap*$^{-/-}$ cells was not sufficient to deplete cIAP2 (Varfolomeev et al., 2007), we probed for NF-κB-inducing kinase (NIK) stabilization. We observed a similar elevation of NIK in both WT and *Xiap*$^{-/-}$ cells (Figures S2G and S2H), indicating that activation of the noncanonical NF-κB pathway did not contribute to the differential levels of IL-1β secretion and cell death.

In summary, depletion of cIAP1/cIAP2 was insufficient for IL-1β secretion and cell death to occur when XIAP was present. Depletion of cIAP1/cIAP2 only further promoted both outcomes when XIAP was deleted. We conclude that protection from excessive inflammasome activation and cell death in DCs after TNFR or TLR4 activation is predominantly mediated by XIAP.

RIP3 Is Required for Cell Death and Inflammasome Activation in *Xiap*$^{-/-}$ BMDCs after TNF/TNFR or TLR4 Stimulation

RIP3 is a mediator of TNF-induced cell death and inflammation (Murphy and Silke, 2014; Vandenabeele et al., 2010). We therefore determined the requirement for RIP3 for both outcomes in XIAP-deficient cells by crossing *Xiap*$^{-/-}$ mice with *Rip3*$^{-/-}$ mice (Newton et al., 2004). *Rip3*$^{-/-}$*Xiap*$^{-/-}$ BMDCs differentiated normally in culture (Figure S3A). After stimulation with TNF (Figure 3A) or LPS (Figures S3B and S3C), the secretion of processed IL-1β into the medium observed in *Xiap*$^{-/-}$ cells was completely abolished by loss of RIP3. The reduction in IL-1β levels correlated with normal cell survival in response to TNF or LPS, implying that inflammasome formation and cell death signaling are both consequences of RIP3 activity (Figures 3A and S3C). Surprisingly, processing of caspase-8 into the p17 subunit was absent in *Rip3*$^{-/-}$*Xiap*$^{-/-}$ BMDCs after TNF or LPS treatment (Figures 3B and S3B). In addition, deletion of

(B) Secreted IL-1β, cell viability, and LDH release of WT and *Xiap*$^{-/-}$ BMDCs treated with LPS (5 ng/ml).

(C) Immunoblotting of cell lysates and culture media from WT and *Xiap*$^{-/-}$ BMDCs treated with LPS (5 ng/ml).

(D) Immunoblotting of NP-40 insoluble fractions isolated from BMDCs after treatment with LPS (5 ng/ml) for 8 hr, or treatment with LPS for 2 hr plus ATP (5 mM) for 1 hr.

(E) Fluorescence microscopy of ASC/caspase-1 specks in WT and *Xiap*$^{-/-}$ BMDCs treated as indicated. Cells were stained for caspase-1 (yellow), nuclei (blue), and vimentin (red). Scale bars represent 20 μm.

(F and G) IL-1β from peritoneal fluid of WT and *Xiap*$^{-/-}$ mice injected with (F) LPS (1 μg) or (G) alum crystals (700 μg) i.p. for 2 hr. n, number of mice.

Error bars represent mean ± SEM. Other data represent mean ± SEM of at least three independent experiments performed in triplicates. See also Figure S1.

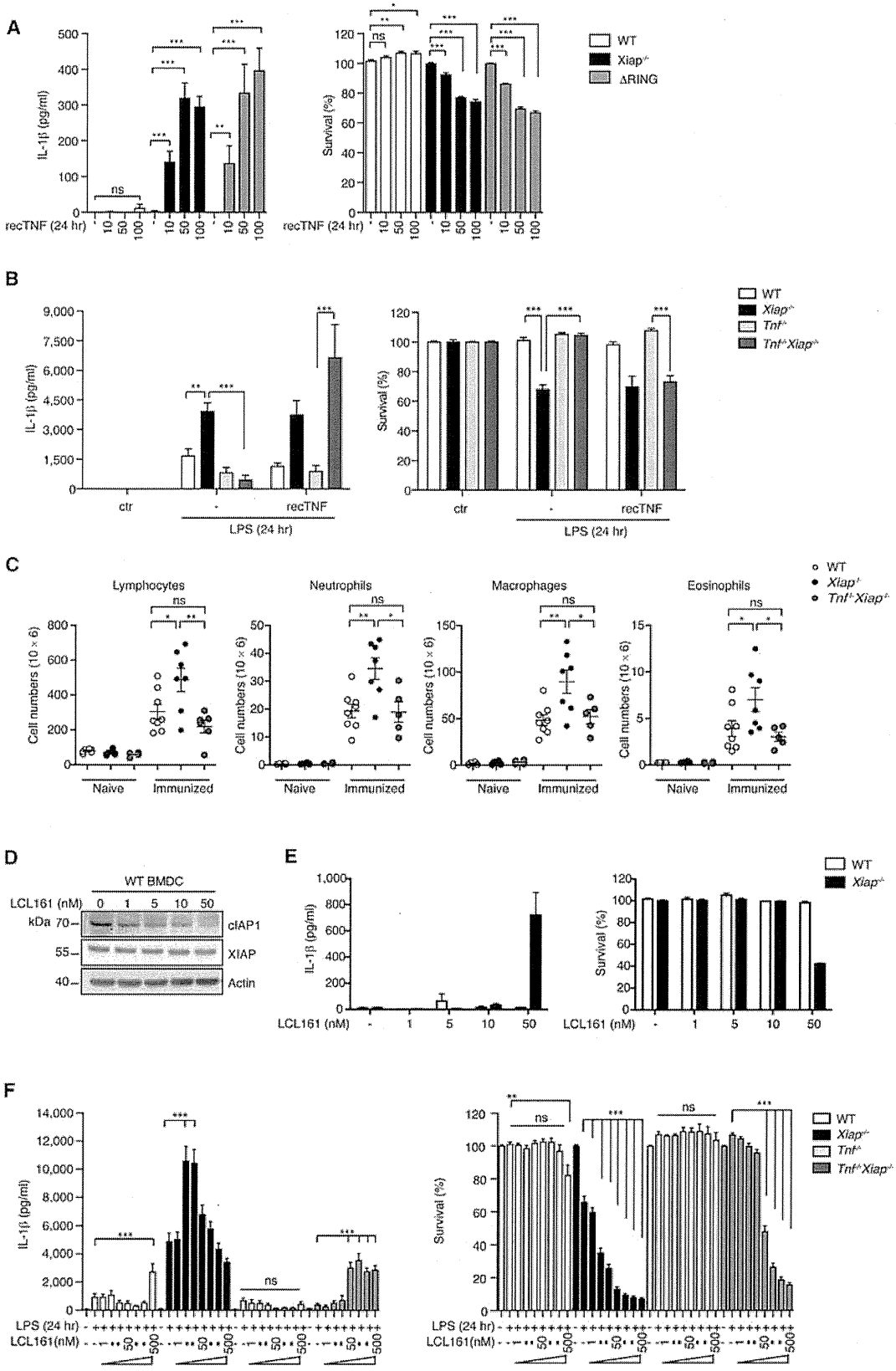

(legend on next page)

Rip3 blocked inflammasome formation as measured by assembly of ASC and caspase-1 within the NP-40 fraction (Figure 3C). The critical role of RIP3 was also confirmed in vivo, where the amount of IL-1β induced by LPS in *Xiap*$^{-/-}$ mice was reduced in *Rip3*$^{-/-}$*Xiap*$^{-/-}$ mice (Figure 3D). These findings identify XIAP as a negative regulator of RIP3-dependent signaling in response to TNF or LPS and detect a critical role for RIP3 in the full activation of caspase-8 in this process.

XIAP Regulates Ubiquitylation of RIP1 outside the TNF-RSC

The finding that XIAP restricted inflammasome activation and cell death downstream of TNF/TNFR signaling prompted us to investigate the impact of XIAP loss on the formation of the TNF-RSC. We performed immunoprecipitations of the TNF-RSC using FLAG-tagged TNF in WT or *Xiap*$^{-/y}$ HCT116 human colorectal carcinoma cells, which have previously been shown to fully form the TNF-RSC and propagate XIAP-dependent signaling (Damgaard et al., 2012; Krieg et al., 2009). We observed no differences in the composition or the ubiquitylation of proteins within the TNF-RSC when XIAP was absent (Figure S3D). This is in line with our data that showed no significant changes in NF-κB and MAPK activation, and gene induction, in *Xiap*$^{-/-}$ and *Xiap*$^{\Delta RING}$ BMDCs after TNF treatment (Figures S2C and S2D).

We next tested whether XIAP alters RIP1 expression by probing for the mRNA and protein levels of RIP1 in BMDCs. No significant changes were observed for RIP1 mRNA in response to either LPS or TNF (Figure S3E). However, compared to WT BMDCs, we observed elevated RIP1 protein levels in *Xiap*$^{-/-}$ cells at baseline and after 8 hr of LPS treatment (Figure 3E). The baseline elevation of RIP1 and the levels after stimulation were dependent on TNF signaling because RIP1 levels were lower in *Tnf*$^{-/-}$*Xiap*$^{-/-}$ cells (Figure 3E). The differences in protein levels despite normal mRNA expression suggest that XIAP affects RIP1 in a posttranslational manner.

We therefore examined whether changes in the ubiquitylation of RIP1 account for its increase. To pull down polyubiquitin chains from BMDCs, we utilized tandem ubiquitin binding entities (TUBEs) fused to glutathione S-transferase (GST). Intriguingly, we found that RIP1 ubiquitylation was substantially elevated after 30 and 60 min of TNF treatment in *Xiap*$^{-/-}$ BMDCs (Figure 3F). This finding was surprising because our data did not show an increase of ubiquitin on RIP1 within the TNF-RSC (Figure S3D) and because depletion of cIAP1/cIAP2 by SMAC mimetics reduces RIP1 ubiquitylation (Bertrand et al., 2008). These data therefore suggest that XIAP regulates RIP1 ubiquitylation independently from cIAP1/cIAP2 and outside the TNF-RSC.

We next investigated whether RIP3 contributes to the ubiquitylation of RIP1, possibly in a RIP1-RIP3-containing protein complex (Cho et al., 2009; Feoktistova et al., 2011; Tenev et al., 2011). We found that genetic deletion of RIP3 completely blocked the aberrant RIP1 ubiquitylation observed in *Xiap*$^{-/-}$ cells (Figure 3G). Collectively, these data show that XIAP contributes to the regulation of the ubiquitylation status of RIP1 in a RIP1-RIP3-containing complex outside of the TNF-RSC I.

Cell Death Is Induced Independently of Inflammasome Activation in *Xiap*$^{-/-}$ BMDCs

The critical role of RIP3 for the inflammasome activation and cell death induction in *Xiap*$^{-/-}$ cells prompted us to examine the relationship between both outcomes. We therefore generated *Caspase 1/11*$^{-/-}$*Xiap*$^{-/-}$ mice (Kuida et al., 1995). In line with previous literature, canonical inflammasome activation induced by ATP was completely blocked in BMDCs from such mice (Figures S4A and S4B).

After LPS treatment, we found a substantial reduction in IL-1β levels in *Caspase 1/11*$^{-/-}$*Xiap*$^{-/-}$ mice compared to *Xiap*$^{-/-}$ mice, implicating conventional inflammasome formation in this process (Figures 4A–4C). Interestingly, IL-1β levels in *Caspase 1/11*$^{-/-}$*Xiap*$^{-/-}$ mice at 24 hr were still substantially elevated compared to WT cells (Figure 4C). This suggested that processing of pro-IL-1β by caspase-8 might cooperate with caspase-1 for IL-1β maturation. Indeed, *Caspase 1/11*$^{-/-}$*Xiap*$^{-/-}$ BMDCs retained the elevated caspase-8 activity also observed in *Xiap*$^{-/-}$ cells (Figures 4A and 4B). Moreover, inhibition of caspase-8 with the inhibitor Z-IETD-FMK (IETD) further reduced IL-1β levels at 8 and 24 hr (Figures 4B and 4C), implying that caspase-8 contributes to IL-1β maturation in *Xiap*$^{-/-}$ BMDCs. We therefore tested the recruitment of both caspases into the NP-40 fraction in response to LPS. We observed that LPS treatment was sufficient to cause recruitment of caspase-8 and caspase-1 into this fraction in *Xiap*$^{-/-}$ cells, whereas WT cells required canonical inflammasome activation with ATP for this to occur (Figures 1D, 3C, and 4D). Of note, recruitment of caspase-8 to the NP-40 fraction was unperturbed in mice lacking caspase-1/caspase-11 (Figure 4D). In addition, inhibition of caspase-8 with IETD did not prevent caspase-1 recruitment to the NP-40 fraction in *Xiap*$^{-/-}$ cells (Figure 4E). Collectively, these data show that recruitment and activation of caspase-1 and caspase-8 occur independently of each other but that both cooperate in the processing of pro-IL-1β.

Importantly, we observed no effect of deletion of caspase-1/caspase-11 on the cell death of *Xiap*$^{-/-}$ cells (Figures 4B and 4C). Additional inhibition of caspase-8 (Figures 4B and 4C) and complete inhibition of all caspase activity using the caspase

Figure 2. XIAP Protects against Excessive IL-1β Secretion and Cell Death in a TNF-Dependent Manner

(A) IL-1β and cell survival of WT, *Xiap*$^{-/-}$, and *Xiap*$^{\Delta RING}$ BMDCs treated with recombinant TNF (recTNF) at 10, 50, and 100 ng/ml.

(B) IL-1β and cell viability of WT, *Xiap*$^{-/-}$, *Tnf*$^{-/-}$, and *Tnf*$^{-/-}$*Xiap*$^{-/-}$ BMDCs after LPS (5 ng/ml) with or without recTNF (100 ng/ml).

(C) Splenic lymphocytes, neutrophils, macrophages, and eosinophils from WT (n = 8), *Xiap*$^{-/-}$ (n = 7), and *Tnf*$^{-/-}$*Xiap*$^{-/-}$ (n = 5) mice 12 days after injection i.p. with coated alum crystals. Each dot represents a mouse, and error bars represent mean ± SEM.

(D) Immunoblots of WT BMDCs treated with IAP antagonist LCL161 for 2 hr.

(E) IL-1β and cell survival of WT and *Xiap*$^{-/-}$ BMDCs after LCL161 for 24 hr.

(F) IL-1β and cell viability of WT, *Xiap*$^{-/-}$, *Tnf*$^{-/-}$, and *Tnf*$^{-/-}$*Xiap*$^{-/-}$ BMDCs after LPS and LCL161 at 1, 5, 10, 50, 100, 200, and 500 nM for 24 hr.

Error bars represent mean ± SEM of at least three independent experiments performed in triplicates. See also Figure S2.

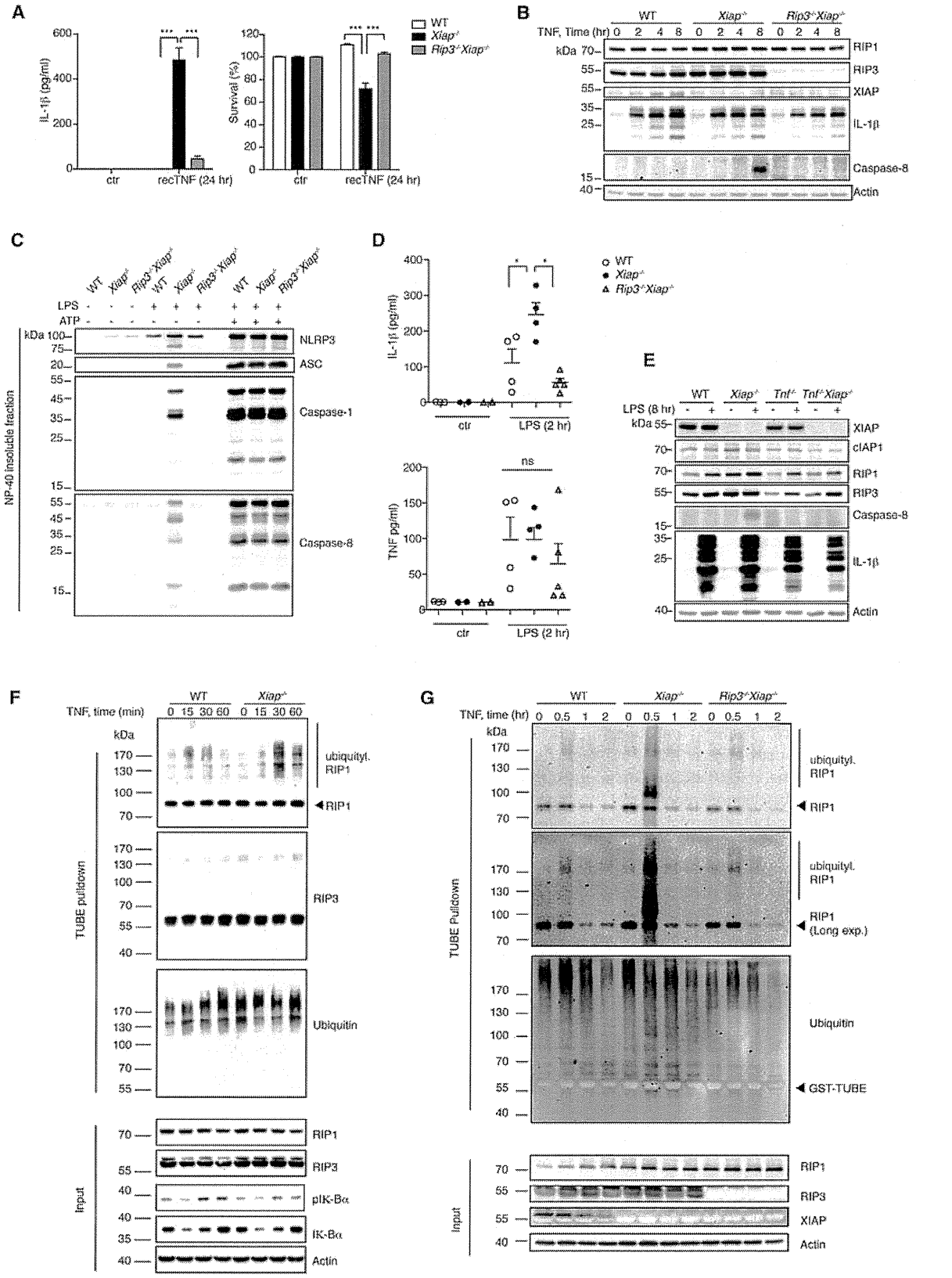

(legend on next page)

inhibitor ZVAD also failed to rescue the viability of *Xiap*$^{-/-}$ cells (Figure S4C). Whereas the precise function of caspase-8 in this context remains unresolved, our data clearly showed that cell death induction was nonapoptotic and independent from inflammasome activation.

Loss of XIAP Drives Excessive Inflammation in a Murine Model of EBV Mononucleosis

XLP-2 pathology in patients is often triggered by an Epstein-Barr virus (EBV) infection. As a murine model for EBV mononucleosis, we studied the immune response of *Xiap*$^{-/-}$ mice to murine γ-herpesvirus 68 (MHV-68) (Barton et al., 2011). In this model, intranasal (i.n.) infection with MHV-68 results in a productive infection of the respiratory tract (Stevenson and Efstathiou, 2005) that is followed by the transfer of the infection to lymphoid tissues. Latent infection is established in the spleen within 2–3 weeks postinfection (p.i.), after which the number of latently infected splenocytes returns to basal levels (Barton et al., 2011) (Figure 5A).

Despite normal viral clearance during early infection (days 6 and 16) (Figure 5B; data not shown), we found increased viral genomic loads in the spleens of infected *Xiap*$^{-/-}$ mice during late (day 43) and very late (day 84) latency (Figure 5B). On day 16, the cellularity of *Xiap*$^{-/-}$ and *Xiap*$^{\Delta RING}$ spleens was increased compared to those of WT mice, which was reflected by the increased numbers of myeloid and lymphoid populations in the spleen (Figure 5C). Because CD4$^+$ T lymphocytes are important for the regulation of the viral loads of MHV-68, we measured T cell populations during active infection and early latency (Figure 5D). Despite equivalent values on day 6 p.i., the levels of CD4$^+$ effector T cells, regulatory T cells (Treg), and IFNγ$^+$ T cells were substantially elevated in *Xiap*$^{-/-}$ and *Xiap*$^{\Delta RING}$ mice at day 16 p.i., a phenotype also observed in patients with XLP-2 (Figure 5D).

In line with our in vitro data, we found substantially elevated IL-1β levels in the peripheral blood of *Xiap*$^{-/-}$ mice at day 16 p.i., whereas TNF was comparable between both genotypes (Figure 5E). Together, this shows that γ-herpesvirus infection drives hyperinflammation in *Xiap*$^{-/-}$ mice, similar to what is seen in EBV-infected patients with XLP-2.

Based on our findings showing the TNF-dependent nature of the excessive IL-1β secretion in *Xiap*$^{-/-}$ BMDCs and mice, we hypothesized that deletion of TNF would ameliorate some of the phenotypes observed. Indeed, during early infection at day 6 p.i., *Tnf*$^{-/-}$*Xiap*$^{-/-}$ mice failed to induce IL-1β induction, whereas at day 16 p.i., stimuli other than TNF induced IL-1β production comparable to the levels observed in *Xiap*$^{-/-}$ mice (Figure 5E). Consistently, we observed a reduction in myeloid and lymphoid subpopulations infiltrating the spleen in *Tnf*$^{-/-}$*Xiap*$^{-/-}$ mice at day 16 p.i. (Figures 5F and 5G). Finally, in agreement with our previous data, deletion of RIP3 also reduced the cellular infiltrations observed in spleens of *Xiap*$^{-/-}$ mice after viral infection (Figure S5A), further supporting a role for RIP3-dependent cell death and inflammation observed in *Xiap*$^{-/-}$ mice.

In summary, the phenotype observed in *Xiap*$^{-/-}$ and *Xiap*$^{\Delta RING}$ mice mimicked XLP-2 pathology, which is characterized by the effort of the immune system to clear an infectious pathogen, such as EBV, causing severe hyperinflammation. Importantly, genetic deletion of TNF ameliorated the symptoms, supporting the causative nature of TNF in this process and indicating a potential therapeutic benefit of TNF inhibition for patients with XLP-2 during early infection.

DISCUSSION

Excessive RIP3-dependent cell death has been shown to cause elevated cytokine production and inflammation collectively resulting in severe tissue damage (Murphy and Silke, 2014). This is exemplified, for example, by the development of severe terminal ileitis in Crohn's disease due to necroptosis of Paneth cells (Günther et al., 2011). Necroptosis-inhibiting proteins are therefore critical regulators of tissue homeostasis (Günther et al., 2011; Kang et al., 2013; Welz et al., 2011). Our data identify XIAP as an inhibitor of RIP3-dependent cell death and inflammation and show that loss of XIAP expression in mice causes hyperinflammation that mimics human XLP-2 pathology (Marsh et al., 2010).

Unexpectedly, our data place XIAP downstream of TNF signaling, despite the fact that it is not directly involved in the formation of the TNF-RSC I. The role of XIAP in TNFR signaling has mainly been characterized in mouse embryonic fibroblasts (MEFs). Contrary to cIAP1, XIAP is not involved in propagating canonical NF-κB activation in response to TNF in MEFs (Moulin et al., 2012) and fails to increase retention of RIP1 within the TNF signaling complex I (Vince et al., 2007). In contrast, our data place XIAP's function outside of the TNF-RSC I, where it controls the cellular fate of DCs by regulating RIP1 ubiquitylation together with RIP3 within a TNF/TNFR-induced signaling complex IIb (also termed ripoptosome or necrosome) (Murphy and Silke, 2014; Tenev et al., 2011). Whether XIAP directly interacts with RIP1 and/or RIP3 or whether the aberrant ubiquitylation of

Figure 3. TNF Induces Elevated Ubiquitylation of RIP1 and Drives RIP3-Dependent Inflammasome Formation and Cell Death in *Xiap*$^{-/-}$ Mice

(A) IL-1β secretion and survival of WT, *Xiap*$^{-/-}$, and *Rip3*$^{-/-}$*Xiap*$^{-/-}$ BMDCs treated with TNF (100 ng/ml). Data represent mean ± SEM of at least three independent experiments performed in triplicates.

(B) Immunoblots of WT, *Xiap*$^{-/-}$, and *Rip3*$^{-/-}$*Xiap*$^{-/-}$ BMDCs treated with TNF (100 ng/ml).

(C) Immunoblots of NP-40 insoluble fractions of WT, *Xiap*$^{-/-}$, and *Rip3*$^{-/-}$*Xiap*$^{-/-}$ BMDCs after LPS (5 ng/ml) for 8 hr, or LPS (10 ng/ml) primed for 2 hr plus ATP (5 mM) for 1 hr.

(D) Cytokines from peritoneal fluid of WT (n = 4), *Xiap*$^{-/-}$ (n = 4), and *Rip3*$^{-/-}$*Xiap*$^{-/-}$ (n = 5) mice after 2 hr of LPS (1 μg) i.p. Each data point represents one mouse. Error bars represent mean ± SEM.

(E) Immunoblots of extracts from WT, *Xiap*$^{-/-}$, *Tnf*$^{-/-}$, and *Tnf*$^{-/-}$*Xiap*$^{-/-}$ BMDCs after treatment with LPS (5 ng/ml).

(F) Immunoblots of GST-TUBE ubiquitin pull-down from WT and *Xiap*$^{-/-}$ BMDCs treated with TNF (100 ng/ml).

(G) Immunoblots of GST-TUBE ubiquitin pull-down from WT, *Xiap*$^{-/-}$, and *Rip3*$^{-/-}$ *Xiap*$^{-/-}$ BMDCs treated with TNF (100 ng/ml).

See also Figure S3.

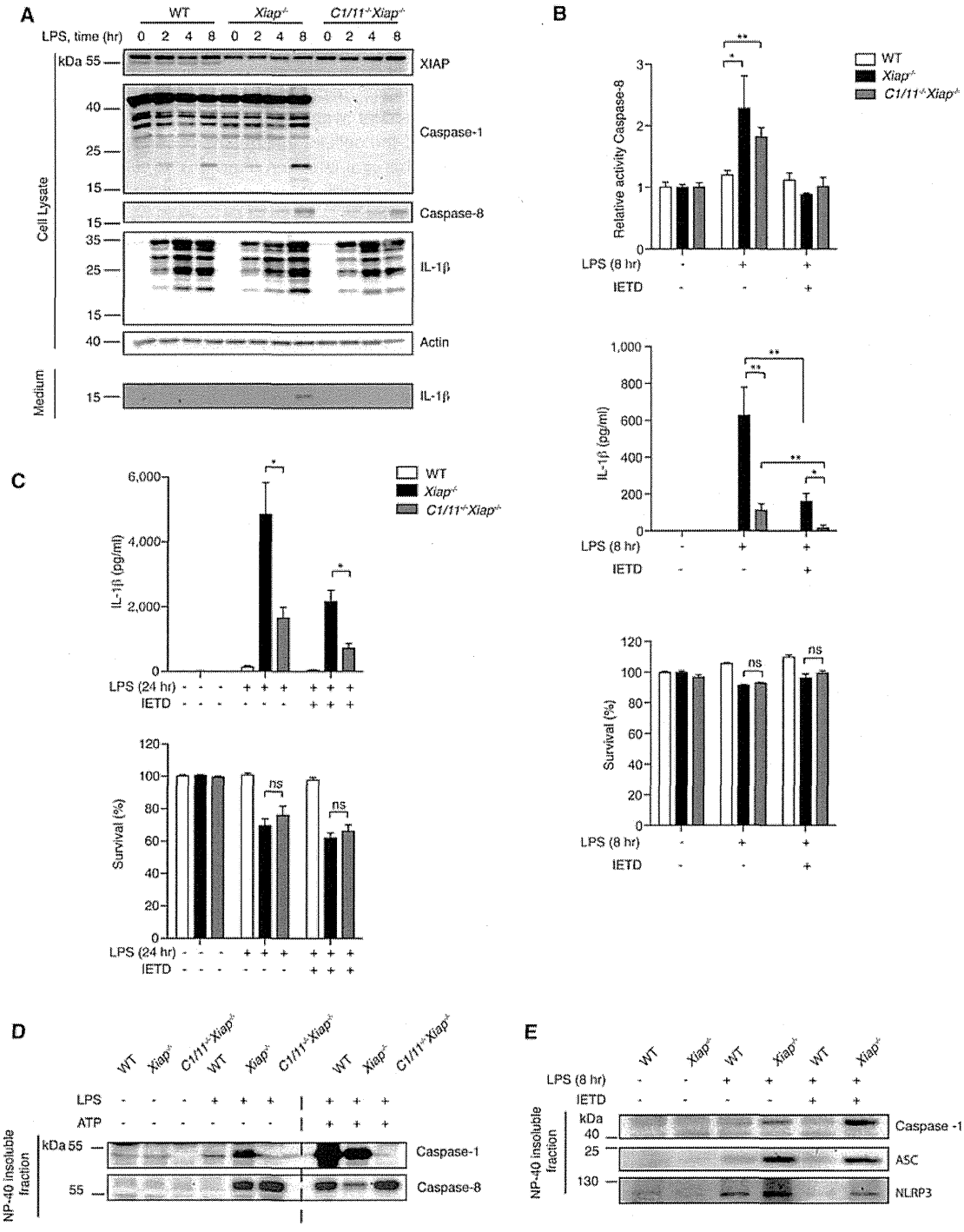

Figure 4. Caspase-1/Caspase-11 and Partially Caspase-8 Drive IL-1β Processing in *Xiap*$^{-/-}$ Mice, but Both Are Dispensable for Cell Death

(A) Immunoblots of cell extracts and media from WT, *Xiap*$^{-/-}$, and *Caspase 1/11*$^{-/-}$*Xiap*$^{-/-}$ BMDCs treated with LPS (5 ng/ml).

(B and C) Relative caspase-8 activity, IL-1β secretion, and survival of WT, *Xiap*$^{-/-}$, and *Caspase 1/11*$^{-/-}$*Xiap*$^{-/-}$ BMDCs after LPS (5 ng/ml) with or without the caspase-8 inhibitor IETD-fmk (IETD) (10 μM) for (B) 8 hr or (C) 24 hr.

(D) NP-40 insoluble fractions of WT, *Xiap*$^{-/-}$, and *Caspase 1/11*$^{-/-}$*Xiap*$^{-/-}$ BMDCs after LPS (5 ng/ml) for 8 hr, or LPS for 2 hr (10 ng/ml) plus ATP (5 mM) for 1 hr.

(E) NP-40 fractions of WT and *Xiap*$^{-/-}$ BMDCs with LPS (5 ng/ml) for 8 hr with or without IETD.

Error bars represent mean ± SEM of at least three independent experiments performed in triplicates. See also Figure S4.

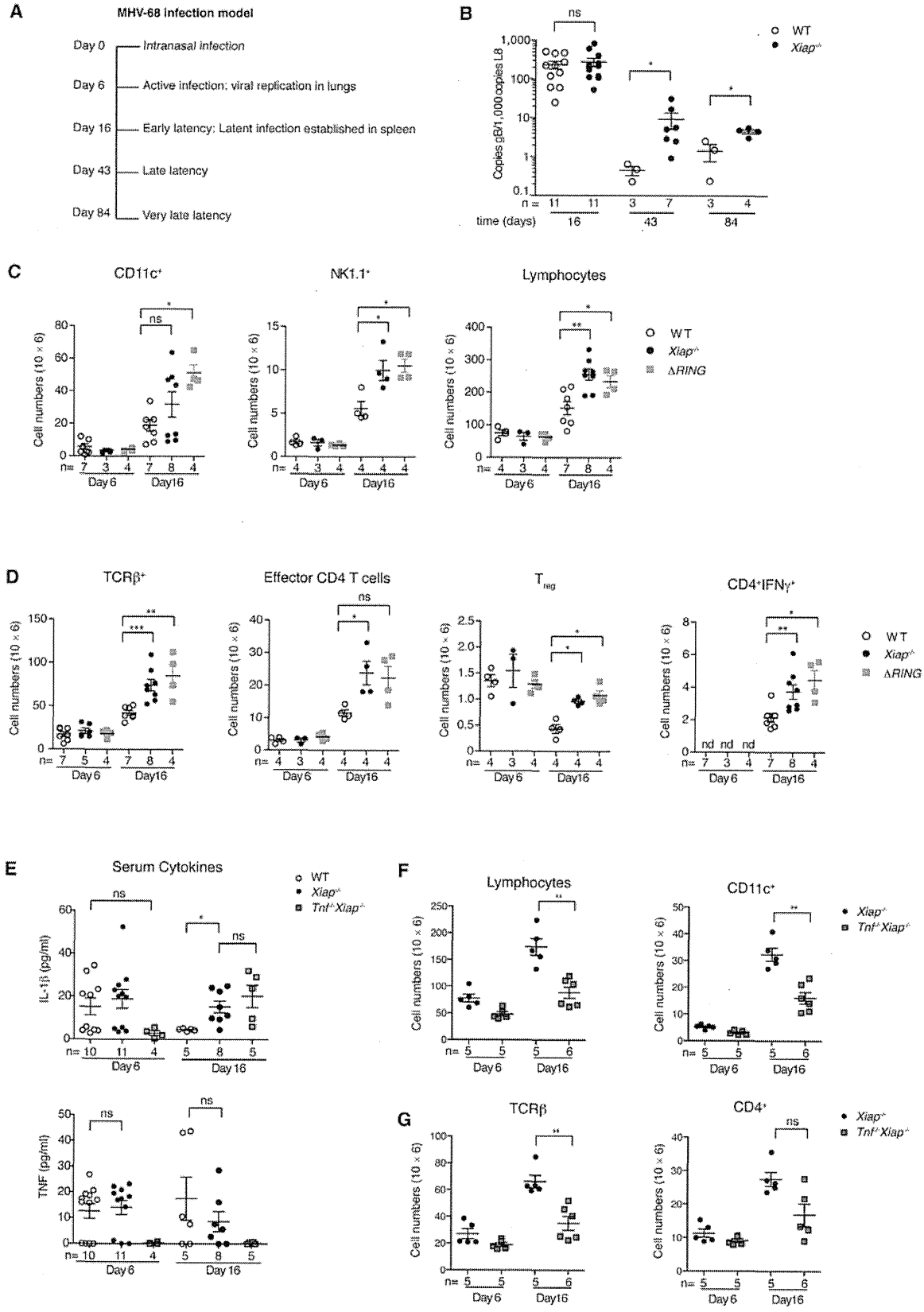

(legend on next page)

RIP1 favors binding to RIP3 remains unresolved, and these questions will be important to further investigate in the future.

The ubiquitylation status of RIP1 is a key factor that influences the switch between cell survival, apoptosis and RIP3-dependent cell death downstream of the TNFR. RIP1 has been shown to be decorated with M1, K11-, K48-, and K63-linked ubiquitin chains (Bertrand et al., 2011; Gerlach et al., 2011; Haas et al., 2009). cIAP1/cIAP2 have been implicated as mediators of the K48 and K63 linkages (Bertrand et al., 2011). Loss of these K48/K63 linkages, either via the action of specific deubiquitinases (DUBs) or by IAP antagonists, leads to cell death (Feoktistova et al., 2011; O'Donnell et al., 2011), whereas loss of the linear M1 linkage attenuates the NK-κB transcriptional response also resulting in elevated cell death (Gerlach et al., 2011; Haas et al., 2009; Ikeda et al., 2011). *Xiap*$^{\Delta RING}$ mutant mice, which express a truncated XIAP missing only the ligase function, presented with an almost identical phenotype compared to *Xiap*$^{-/-}$ mice. This supports the notion that XIAP functions as a ubiquitin ligase in TNFR/TNF signaling and that coordinated ubiquitylation events downstream of TNFR are tightly controlled by IAPs, including XIAP.

We observed an aberrant and prolonged ubiquitylation of RIP1 after TNF stimulation in cells lacking XIAP. Our data argue that XIAP functions as a ubiquitin ligase controlling the ubiquitylation of RIP1 either directly or indirectly, e.g., by affecting another ubiquitin ligase or DUB, which is important for ensuring correct RIP1 ubiquitylation. Indeed, there is emerging evidence that RIP1 ubiquitylation is tightly balanced by multiple ubiquitin ligases and DUBs and that altering this balance results in aberrant signaling and cell death (Gerlach et al., 2011; Keusekotten et al., 2013; O'Donnell et al., 2011; Wertz et al., 2004).

We show that XIAP cooperates with cIAP1/cIAP2 in diverging TNFR/TNF signaling away from cell death. However, XIAP clearly functions independently of cIAP1/cIAP2. This is exemplified by the fact that deletion of XIAP alone is sufficient to drive the observed phenotype and by the observation that deletion of XIAP causes aberrantly elevated ubiquitylation of RIP1 instead of the reduced RIP1 ubiquitylation observed when cIAP1/cIAP2 are inhibited (Bertrand et al., 2008)

XLP-2 is currently considered a familial hemophagocytic lymphohistiocytosis (HLH) disease despite the lack of the characteristic defects of CD8$^+$ T cell and natural killer cell cytotoxicity usually present in familial patients with HLH (Marsh et al., 2010). The protection of DCs and macrophages against RIP3-dependent cell death and inflammation afforded by XIAP argues that loss-of-function mutations constitute a major underlying cause of XLP-2 pathology. TNF was identified as the prime causative cytokine in our study, and genetic inhibition ameliorated some disease-specific symptoms. Despite the likely contribution of alternative inflammatory pathways, such as IFN signaling, we suggest that patients with XLP-2 might profit from therapeutic TNF inhibition when used early during an inflammatory episode (Mischler et al., 2007).

EXPERIMENTAL PROCEDURES

Mice

Xiap$^{-/-}$ (Olayioye et al., 2005) and *Xiap*$^{\Delta RING}$ (Schile et al., 2008) mice have been previously described. *Tnf tm1Gkl* (*Tnf*$^{-/-}$) (Pasparakis et al., 1996) and *Casp1*^{tm1Flv}*/J* (*Caspase-1/Caspase-11*$^{-/-}$) (Kuida et al., 1995) mice were purchased from Jackson Laboratories. *Rip3*$^{-/-}$ mice were obtained under a material transfer agreement from Genentech and have been previously described by Newton et al. (2004). Both male and female mice deficient for *BIRC4* were denoted *Xiap*$^{-/-}$. All animal experiments were performed in compliance with protocols approved by the local animal ethics committee guidelines.

Inflammasome Formation in BMDCs

To monitor inflammasome formation by fluorescence microscopy, cells treated with or without nigericin (5 μM) (Sigma-Aldrich) for 20–30 min after LPS priming for 2 hr were seeded on chamber slides and probed with antibodies against caspase-1 (Casper-2 clone; Adipogen) and vimentin (D21H3; Cell Signaling Technology). Images were acquired with a Leica DMRBE fluorescence microscope. For inflammasome-enrichment studies, cells were treated with LPS or TNF for the indicated times, and the insoluble fraction of the NP-40-lysed cells was collected by centrifugation and analyzed by SDS-PAGE and immunoblotting for ASC, caspase-1 (Casper-1 clone), as previously described (Gross et al., 2012).

Alum-Induced Peritonitis and Immunization

Eight to 12-week-old age- and sex-matched mice were injected i.p. with 700 μg Imject Alum Adjuvant (Thermo Scientific) in 200 μl PBS. Peritoneal fluid was collected 2 hr postinjection and concentrated to 100 μl with 10 kDa MWCO Vivaspin filters (Vivascience), and cytokines were measured by Cytokine Bead Array (BD Biosciences). For immunization, ovalbumin (100 μg) (Sigma-Aldrich; A2512) and LPS (10 μg) (Sigma-Aldrich; L2880) were precipitated with alum (4.4 μg) (Roth P724.1). Each mouse was injected with the precipitate that was washed once with PBS. Spleens of mice were analyzed by flow cytometry 12 days later.

Intranasal MHV-68 Infection

Intranasal (i.n) infection of mice was performed as previously described by El-Gogo et al. (2007) and Stevenson and Efstathiou (2005). In brief, mice were infected i.n. with 5×10^4 plaque-forming units. Lytic virus titers of infected lungs were determined on day 6, and splenic latent viral load was performed by real-time PCR. At days 6 and 16 p.i., spleens of infected mice were analyzed by flow cytometry analysis, and cytokines were measured from blood sera.

Statistical Analyses

The Wilcoxon-Mann-Whitney test was used to compare levels of serum cytokines and differences in cellular populations. All values are expressed as the mean ± SEM, and $p < 0.05$ (*), $p < 0.005$ (**), and $p < 0.0005$ (***) were

Figure 5. *Xiap*$^{-/-}$ and *Xiap*$^{\Delta RING}$ Mice Infected with MHV-68 Develop Excessive Inflammation

(A) Schematic overview of the MHV-68 infection model.

(B) MHV-68 viral genomic load of spleens from infected WT and *Xiap*$^{-/-}$ mice determined on days 16, 43, and 84 p.i.

(C) Flow cytometric analyses of spleens of infected WT, *Xiap*$^{-/-}$, and *Xiap*$^{\Delta RING}$ mice were analyzed at days 6 and 16 p.i.

(D) T cell subsets of infected mice were analyzed as in (C). Effector T cells were defined as TCRβ$^+$, CD4$^+$, CD44^{high}, CD62L^{low}, and T-regs as CD4$^+$, CD25$^+$, and FOXP3$^+$.

(E) IL-1β and TNF from sera of infected WT, *Xiap*$^{-/-}$, and *Tnf*$^{-/-}$*Xiap*$^{-/-}$ mice at days 6 and 16 p.i.

(F) Flow cytometric analysis of spleens of infected *Xiap*$^{-/-}$ and *Tnf*$^{-/-}$*Xiap*$^{-/-}$ mice at days 6 and 16 p.i.

(G) T cell numbers from mice in (F).

Each dot represents a mouse, and error bars represent mean ± SEM. See also Figure S5.

considered statistically significant. Statistical analyses and graphing were performed with GraphPad Prism software.

SUPPLEMENTAL INFORMATION

Supplemental Information includes Supplemental Experimental Procedures and five figures and can be found with this article online at http://dx.doi.org/10.1016/j.celrep.2014.05.008.

AUTHOR CONTRIBUTIONS

P.J.J. conceived and supervised the project, analyzed the data, and wrote the manuscript. M.Y. conceived and performed the experiments, analyzed the data, and wrote the manuscript. N.M., H.A., N.K., C.J.G., R.B.D., and O.G. performed experiments. H.K., M.R., and M.G.-H. provided critical reagents and samples. T.K., M.H., A.S., J.R., O.G., C.P., and M.G.-H. gave conceptual advice and wrote the paper.

ACKNOWLEDGMENTS

We thank H. Steller, C. Borner, D. Vaux, D. Porter, B. Vogelstein, L. O'Reilly, and Genentech and Novartis for gifts of mice and reagents; S. Rott, H. Bendz, J. Christian, D. Kull, R. Hillermann, B. Steer, and M. Strehle for excellent technical assistance; and R. Holmes (Berlin) for language support. P.J.J. was supported by a Max Eder-Program grant from the Deutsche Krebshilfe (program #109310), a Human Frontiers Science Program grant (program #RGY0073/2012), and the German Jose Carreras Leukemia Foundation grant (DJCLS R 12/22). H.A. was supported by grants from Wilhelm Sander-Stiftung (2009.046.1+2) and the BMBF (NGFNplus, PIM-01GS0802-3). M.H. was supported by the Helmholtz-Foundation and the Peter-Hans Hofschneider Foundation. N.M. and C.J.G. are members of the TUM Graduate School. C.J.G. is supported by the Natural Science and Engineering Research Council of Canada. O.G. is supported by the Bavarian Molecular Biosystems Research Network. M.G.-H. is supported by a Steno Fellowship from the Danish Council for Independent Research-Natural Sciences, the Lundbeck Foundation, and the Novo Nordisk Foundation.

Received: September 24, 2013
Revised: April 10, 2014
Accepted: May 5, 2014
Published: May 29, 2014

REFERENCES

Barton, E., Mandal, P., and Speck, S.H. (2011). Pathogenesis and host control of gammaherpesviruses: lessons from the mouse. Annu. Rev. Immunol. *29*, 351–397.

Bauler, L.D., Duckett, C.S., and O'Riordan, M.X. (2008). XIAP regulates cytosol-specific innate immunity to Listeria infection. PLoS Pathog. *4*, e1000142.

Bertrand, M.J., Milutinovic, S., Dickson, K.M., Ho, W.C., Boudreault, A., Durkin, J., Gillard, J.W., Jaquith, J.B., Morris, S.J., and Barker, P.A. (2008). cIAP1 and cIAP2 facilitate cancer cell survival by functioning as E3 ligases that promote RIP1 ubiquitination. Mol. Cell *30*, 689–700.

Bertrand, M.J., Lippens, S., Staes, A., Gilbert, B., Roelandt, R., De Medts, J., Gevaert, K., Declercq, W., and Vandenabeele, P. (2011). cIAP1/2 are direct E3 ligases conjugating diverse types of ubiquitin chains to receptor interacting proteins kinases 1 to 4 (RIP1-4). PLoS One *6*, e22356.

Cho, Y.S., Challa, S., Moquin, D., Genga, R., Ray, T.D., Guildford, M., and Chan, F.K. (2009). Phosphorylation-driven assembly of the RIP1-RIP3 complex regulates programmed necrosis and virus-induced inflammation. Cell *137*, 1112–1123.

Damgaard, R.B., Nachbur, U., Yabal, M., Wong, W.W., Fiil, B.K., Kastirr, M., Rieser, E., Rickard, J.A., Bankovacki, A., Peschel, C., et al. (2012). The ubiquitin ligase XIAP recruits LUBAC for NOD2 signaling in inflammation and innate immunity. Mol. Cell *46*, 746–758.

Damgaard, R.B., Fiil, B.K., Speckmann, C., Yabal, M., zur Stadt, U., Bekker-Jensen, S., Jost, P.J., Ehl, S., Mailand, N., and Gyrd-Hansen, M. (2013). Disease-causing mutations in the XIAP BIR2 domain impair NOD2-dependent immune signalling. EMBO Mol. Med. *5*, 1278–1295.

Deveraux, Q.L., Takahashi, R., Salvesen, G.S., and Reed, J.C. (1997). X-linked IAP is a direct inhibitor of cell-death proteases. Nature *388*, 300–304.

Eisenbarth, S.C., Colegio, O.R., O'Connor, W., Sutterwala, F.S., and Flavell, R.A. (2008). Crucial role for the Nalp3 inflammasome in the immunostimulatory properties of aluminium adjuvants. Nature *453*, 1122–1126.

El-Gogo, S., Staib, C., Meyr, M., Erfle, V., Sutter, G., and Adler, H. (2007). Recombinant murine gammaherpesvirus 68 (MHV-68) as challenge virus to test efficacy of vaccination against chronic virus infections in the mouse model. Vaccine *25*, 3934–3945.

Feoktistova, M., Geserick, P., Kellert, B., Dimitrova, D.P., Langlais, C., Hupe, M., Cain, K., MacFarlane, M., Häcker, G., and Leverkus, M. (2011). cIAPs block Ripoptosome formation, a RIP1/caspase-8 containing intracellular cell death complex differentially regulated by cFLIP isoforms. Mol. Cell *43*, 449–463.

Gerlach, B., Cordier, S.M., Schmukle, A.C., Emmerich, C.H., Rieser, E., Haas, T.L., Webb, A.I., Rickard, J.A., Anderton, H., Wong, W.W., et al. (2011). Linear ubiquitination prevents inflammation and regulates immune signalling. Nature *471*, 591–596.

Gross, O., Yazdi, A.S., Thomas, C.J., Masin, M., Heinz, L.X., Guarda, G., Quadroni, M., Drexler, S.K., and Tschopp, J. (2012). Inflammasome activators induce interleukin-1α secretion via distinct pathways with differential requirement for the protease function of caspase-1. Immunity *36*, 388–400.

Günther, C., Martini, E., Wittkopf, N., Amann, K., Weigmann, B., Neumann, H., Waldner, M.J., Hedrick, S.M., Tenzer, S., Neurath, M.F., and Becker, C. (2011). Caspase-8 regulates TNF-α-induced epithelial necroptosis and terminal ileitis. Nature *477*, 335–339.

Gyrd-Hansen, M., and Meier, P. (2010). IAPs: from caspase inhibitors to modulators of NF-kappaB, inflammation and cancer. Nat. Rev. Cancer *10*, 561–574.

Haas, T.L., Emmerich, C.H., Gerlach, B., Schmukle, A.C., Cordier, S.M., Rieser, E., Feltham, R., Vince, J., Warnken, U., Wenger, T., et al. (2009). Recruitment of the linear ubiquitin chain assembly complex stabilizes the TNF-R1 signaling complex and is required for TNF-mediated gene induction. Mol. Cell *36*, 831–844.

Ikeda, F., Deribe, Y.L., Skånland, S.S., Stieglitz, B., Grabbe, C., Franz-Wachtel, M., van Wijk, S.J., Goswami, P., Nagy, V., Terzic, J., et al. (2011). SHARPIN forms a linear ubiquitin ligase complex regulating NF-κB activity and apoptosis. Nature *471*, 637–641.

Jordan, M.B., Mills, D.M., Kappler, J., Marrack, P., and Cambier, J.C. (2004). Promotion of B cell immune responses via an alum-induced myeloid cell population. Science *304*, 1808–1810.

Jost, P.J., Grabow, S., Gray, D., McKenzie, M.D., Nachbur, U., Huang, D.C., Bouillet, P., Thomas, H.E., Borner, C., Silke, J., et al. (2009). XIAP discriminates between type I and type II FAS-induced apoptosis. Nature *460*, 1035–1039.

Kang, T.B., Yang, S.H., Toth, B., Kovalenko, A., and Wallach, D. (2013). Caspase-8 blocks kinase RIPK3-mediated activation of the NLRP3 inflammasome. Immunity *38*, 27–40.

Keusekotten, K., Elliott, P.R., Glockner, L., Fiil, B.K., Damgaard, R.B., Kulathu, Y., Wauer, T., Hospenthal, M.K., Gyrd-Hansen, M., Krappmann, D., et al. (2013). OTULIN antagonizes LUBAC signaling by specifically hydrolyzing Met1-linked polyubiquitin. Cell *153*, 1312–1326.

Kool, M., Soullié, T., van Nimwegen, M., Willart, M.A., Muskens, F., Jung, S., Hoogsteden, H.C., Hammad, H., and Lambrecht, B.N. (2008). Alum adjuvant boosts adaptive immunity by inducing uric acid and activating inflammatory dendritic cells. J. Exp. Med. *205*, 869–882.

Krieg, A., Correa, R.G., Garrison, J.B., Le Negrate, G., Welsh, K., Huang, Z., Knoefel, W.T., and Reed, J.C. (2009). XIAP mediates NOD signaling via interaction with RIP2. Proc. Natl. Acad. Sci. USA *106*, 14524–14529.

Kuida, K., Lippke, J.A., Ku, G., Harding, M.W., Livingston, D.J., Su, M.S., and Flavell, R.A. (1995). Altered cytokine export and apoptosis in mice deficient in interleukin-1 beta converting enzyme. Science *267*, 2000–2003.

Lamkanfi, M., and Dixit, V.M. (2012). Inflammasomes and their roles in health and disease. Annu. Rev. Cell Dev. Biol. *28*, 137–161.

Marsh, R.A., Madden, L., Kitchen, B.J., Mody, R., McClimon, B., Jordan, M.B., Bleesing, J.J., Zhang, K., and Filipovich, A.H. (2010). XIAP deficiency: a unique primary immunodeficiency best classified as X-linked familial hemophagocytic lymphohistiocytosis and not as X-linked lymphoproliferative disease. Blood *116*, 1079–1082.

Martinon, F., Burns, K., and Tschopp, J. (2002). The inflammasome: a molecular platform triggering activation of inflammatory caspases and processing of proIL-beta. Mol. Cell *10*, 417–426.

Mischler, M., Fleming, G.M., Shanley, T.P., Madden, L., Levine, J., Castle, V., Filipovich, A.H., and Cornell, T.T. (2007). Epstein-Barr virus-induced hemophagocytic lymphohistiocytosis and X-linked lymphoproliferative disease: a mimicker of sepsis in the pediatric intensive care unit. Pediatrics *119*, e1212–e1218.

Moulin, M., Anderton, H., Voss, A.K., Thomas, T., Wong, W.W., Bankovacki, A., Feltham, R., Chau, D., Cook, W.D., Silke, J., and Vaux, D.L. (2012). IAPs limit activation of RIP kinases by TNF receptor 1 during development. EMBO J. *31*, 1679–1691.

Murphy, J.M., and Silke, J. (2014). Ars Moriendi; the art of dying well - new insights into the molecular pathways of necroptotic cell death. EMBO Rep. *15*, 155–164.

Murphy, J.M., Czabotar, P.E., Hildebrand, J.M., Lucet, I.S., Zhang, J.G., Alvarez-Diaz, S., Lewis, R., Lalaoui, N., Metcalf, D., Webb, A.I., et al. (2013). The pseudokinase MLKL mediates necroptosis via a molecular switch mechanism. Immunity *39*, 443–453.

Newton, K., Sun, X., and Dixit, V.M. (2004). Kinase RIP3 is dispensable for normal NF-kappa Bs, signaling by the B-cell and T-cell receptors, tumor necrosis factor receptor 1, and Toll-like receptors 2 and 4. Mol. Cell. Biol. *24*, 1464–1469.

O'Donnell, M.A., Perez-Jimenez, E., Oberst, A., Ng, A., Massoumi, R., Xavier, R., Green, D.R., and Ting, A.T. (2011). Caspase 8 inhibits programmed necrosis by processing CYLD. Nat. Cell Biol. *13*, 1437–1442.

Olayioye, M.A., Kaufmann, H., Pakusch, M., Vaux, D.L., Lindeman, G.J., and Visvader, J.E. (2005). XIAP-deficiency leads to delayed lobuloalveolar development in the mammary gland. Cell Death Differ. *12*, 87–90.

Pachlopnik Schmid, J., Canioni, D., Moshous, D., Touzot, F., Mahlaoui, N., Hauck, F., Kanegane, H., Lopez-Granados, E., Mejstrikova, E., Pellier, I., et al. (2011). Clinical similarities and differences of patients with X-linked lymphoproliferative syndrome type 1 (XLP-1/SAP deficiency) versus type 2 (XLP-2/XIAP deficiency). Blood *117*, 1522–1529.

Pasparakis, M., Alexopoulou, L., Episkopou, V., and Kollias, G. (1996). Immune and inflammatory responses in TNF alpha-deficient mice: a critical requirement for TNF alpha in the formation of primary B cell follicles, follicular dendritic cell networks and germinal centers, and in the maturation of the humoral immune response. J. Exp. Med. *184*, 1397–1411.

Prakash, H., Albrecht, M., Becker, D., Kuhlmann, T., and Rudel, T. (2010). Deficiency of XIAP leads to sensitization for Chlamydophila pneumoniae pulmonary infection and dysregulation of innate immune response in mice. J. Biol. Chem. *285*, 20291–20302.

Rigaud, S., Fondanèche, M.C., Lambert, N., Pasquier, B., Mateo, V., Soulas, P., Galicier, L., Le Deist, F., Rieux-Laucat, F., Revy, P., et al. (2006). XIAP deficiency in humans causes an X-linked lymphoproliferative syndrome. Nature *444*, 110–114.

Schile, A.J., García-Fernández, M., and Steller, H. (2008). Regulation of apoptosis by XIAP ubiquitin-ligase activity. Genes Dev. *22*, 2256–2266.

Stevenson, P.G., and Efstathiou, S. (2005). Immune mechanisms in murine gammaherpesvirus-68 infection. Viral Immunol. *18*, 445–456.

Tenev, T., Bianchi, K., Darding, M., Broemer, M., Langlais, C., Wallberg, F., Zachariou, A., Lopez, J., MacFarlane, M., Cain, K., and Meier, P. (2011). The Ripoptosome, a signaling platform that assembles in response to genotoxic stress and loss of IAPs. Mol. Cell *43*, 432–448.

Vandenabeele, P., Declercq, W., Van Herreweghe, F., and Vanden Berghe, T. (2010). The role of the kinases RIP1 and RIP3 in TNF-induced necrosis. Sci. Signal. *3*, re4.

Varfolomeev, E., Blankenship, J.W., Wayson, S.M., Fedorova, A.V., Kayagaki, N., Garg, P., Zobel, K., Dynek, J.N., Elliott, L.O., Wallweber, H.J., et al. (2007). IAP antagonists induce autoubiquitination of c-IAPs, NF-kappaB activation, and TNFalpha-dependent apoptosis. Cell *131*, 669–681.

Vince, J.E., Wong, W.W., Khan, N., Feltham, R., Chau, D., Ahmed, A.U., Benetatos, C.A., Chunduru, S.K., Condon, S.M., McKinlay, M., et al. (2007). IAP antagonists target cIAP1 to induce TNFalpha-dependent apoptosis. Cell *131*, 682–693.

Vince, J.E., Wong, W.W., Gentle, I., Lawlor, K.E., Allam, R., O'Reilly, L., Mason, K., Gross, O., Ma, S., Guarda, G., et al. (2012). Inhibitor of apoptosis proteins limit RIP3 kinase-dependent interleukin-1 activation. Immunity *36*, 215–227.

Wada, T., Kanegane, H., Ohta, K., Katoh, F., Imamura, T., Nakazawa, Y., Miyashita, R., Hara, J., Hamamoto, K., Yang, X., et al. (2014). Sustained elevation of serum interleukin-18 and its association with hemophagocytic lymphohistiocytosis in XIAP deficiency. Cytokine *65*, 74–78.

Weisberg, E., Ray, A., Barrett, R., Nelson, E., Christie, A.L., Porter, D., Straub, C., Zawel, L., Daley, J.F., Lazo-Kallanian, S., et al. (2010). Smac mimetics: implications for enhancement of targeted therapies in leukemia. Leukemia *24*, 2100–2109.

Welz, P.S., Wullaert, A., Vlantis, K., Kondylis, V., Fernández-Majada, V., Ermolaeva, M., Kirsch, P., Sterner-Kock, A., van Loo, G., and Pasparakis, M. (2011). FADD prevents RIP3-mediated epithelial cell necrosis and chronic intestinal inflammation. Nature *477*, 330–334.

Wertz, I.E., O'Rourke, K.M., Zhou, H., Eby, M., Aravind, L., Seshagiri, S., Wu, P., Wiesmann, C., Baker, R., Boone, D.L., et al. (2004). De-ubiquitination and ubiquitin ligase domains of A20 downregulate NF-kappaB signalling. Nature *430*, 694–699.

厚生労働科学研究委託費
難治性疾患等実用化研究事業

原発性免疫不全症候群の病態解明と
新規治療法開発への応用に関する研究

平成２６年度委託業務成果報告書

発行日　平成27年3月31日
発行者　野々山　恵章
発行所　厚生労働省難治性疾患等実用化研究事業
原発性免疫不全症候群の病態解明と
新規治療法開発への応用に関する研究
研究代表者　野々山　恵章
〒359-8513
埼玉県所沢市並木３丁目２番地
ＴＥＬ（04）2995-1621
ＦＡＸ（04）2995-5204